Chem, Volume *8*

Supplemental information

Quadrupling the stored charge

by extending the accessible density of states

Mengyu Yan, Peiyao Wang, Xuelei Pan, Qiulong Wei, Chunhua Han, Jefferson Zhe Liu, Yunlong Zhao, Kangning Zhao, Bruce Dunn, Jihui Yang, and Liqiang Mai

Table of Contents

Part 1: Supplemental Experimental Procedures

1. Characterization

X-ray diffraction (XRD) was performed to investigate the crystallographic parameters of the samples. XRD analysis was performed using a Bruker D8 Discover X-ray diffractometer equipped with a Cu Kα X-ray source (λ = 1.5406 Å). Field-emission scanning electron microscope images were collected with a JSM-7001F instrument operated at an acceleration voltage of 10 kV. Transmission electron microscopy (TEM) and high-resolution TEM images were recorded using a JEM-2100F transmission electron microscope equipped with an energy-dispersive X-ray spectrometer.

2. The fitting of X-ray diffraction data

A Lorentzian peak profile was used to model the size broadening. The apparent size is assumed to be isotropic by using a fourth-order spherical harmonics correction with respect to different (hkl) and structure reflections. The dependence of the full width at half maximum, β, on θ is given by

$$\beta = \frac{\lambda}{L \cdot \cos\theta_{hkl}} ,$$

where λ is the wavelength, and L the refined apparent size parameter. Fitting of the powder diffraction patterns between 10° and 80° (2θ) was carried out using the TOPAS structural refinement package.

3. Electrochemical characterization

Cyclic voltammetry (CV) was carried out using an electrochemical workstation (Autolab PGSTAT 302N), with the devices electrically connected to the probe station (Lakeshore TTP4). The stored charge values were calculated from the CV data according to the following equation

$$Q = \frac{1}{v}\int_{V_i}^{V_f} I(V)dV ,$$

where Q is the stored charge of the electrodes, v the scan rate (V/s), V_f and V_i the integration potential limits of the CV curve, and I(V) the discharge current (in Amps). The stored charge per unit area, $Q_{electrode}$ (C/cm^2) of the active material is calculated based on the surface area of the single nanowire/nanosheet, $A_{electrode}$ (cm^2), according to

$$Q_{electrode} = Q/A_{electrode} .$$

For example, the length and diameter of the nanowire we tested for Figure 1c are 21.8 μm and 30 nm, respectively. Thus, the exposed surface area the nanowire is $A_{electrode}$ = length × diameter × π = 2.05 × 10^{-8} cm^2.

We used a MoS_2 sheet prepared by mechanical exfoliation as another example to investigate field-effect energy storage. Similar to the α-MnO_2 single-nanowire FE-ESD, the MoS_2 nanosheet was used as a cathode and with an SU-8 passivation layer. We collected CV curves for the MoS_2 nanosheets at a scan rate of 100 mV/s. The oxidation and reduction peaks are observed at -0.04 and 0.10 V *vs.* SCE, respectively, in the three-electrode system. With an increase of the gate-voltage from 0 to 7 V, an increased stored charge is observed as indicated in the α-MnO_2 FE-ESDs. The anodic/cathodic peak currents increase with the increasing gate-voltage, indicating a greater amount of stored charge. At a scan rate of 100 mV/s, the stored charge of the MoS_2 sheet is 11.4, 25.4, 35.4, 39.8, and 43.6 mC/cm^2 at a gate-voltage of 0, 1, 2, 3, and 4 V, respectively. At a gate-voltage of 4 V, the stored charge is 2 – 4 times higher than without a gate-voltage, regardless of the scan rate. The stored charge saturates as the gate-voltage increases from 4 to 7 V.

4. Understanding the large variation in the reproducibility results

There are three reasons for the large variation in Figure 2d. (1) The diameter of the MnO_2 nanowire determines the stored charge without gate-voltage. Specifically, a larger diameter of MnO_2 will lead to a higher stored charge per area. Thus, a large variation is observed at a gate-voltage of 0 V. (2) The nanowire diameter also influences the profile of the Fermi-level under gate-voltages, which affects the amplifier effect of gate-voltages on the nanowire. As shown in Figure

4e, the band bending gradient of nanomaterials immersed in electrolytes is determined by the following factors, the initial Fermi-levels of the nanomaterial and electrolyte, as well as the carrier density of them. If the nanomaterial size is tiny, which is even smaller than its Debye length, the Fermi-level of the nanomaterial will be significantly tuned by the electrolyte. Thus, leading to a competition between the electrolyte gating and the architecture gating (gate voltage in this manuscript). The profile of the gradient Fermi-level varies with the different thickness/height of the materials, which finally determines its electrochemical charge storage capability. (3) As aforementioned, the initial Fermi-level of nanowires and their carrier density will influence the Fermi-level profile under gate-voltages. Since our nanowire is fabricated with the hydrothermal method, leading to a nanowire-to-nanowire difference in their diameter, Fermi-level position and carrier density. Thus, a large variation is observed in Figure 2d.

Part 2: Supplemental Figures

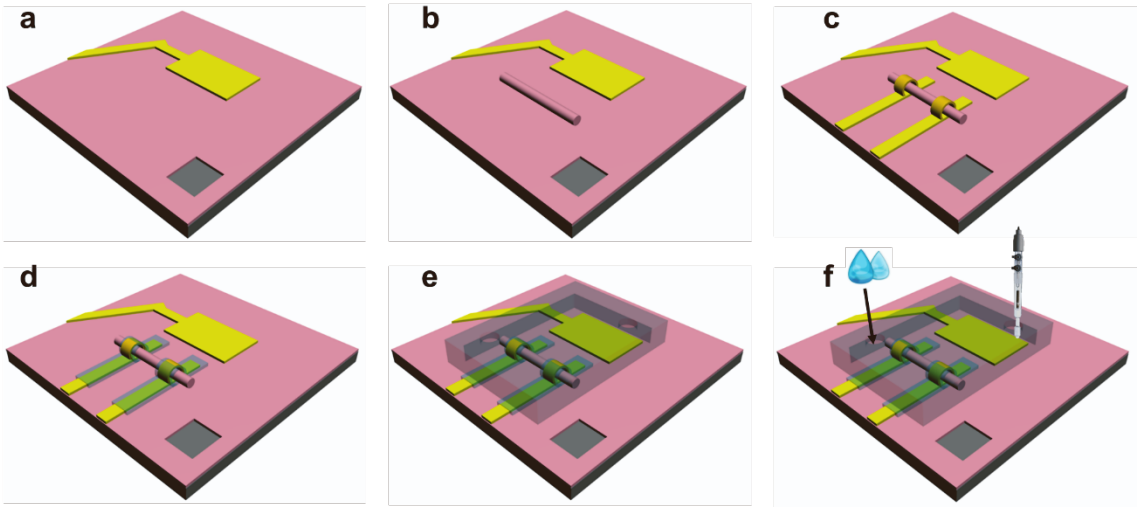

Figure S1. Nanodevice fabrication procedure. **a**. The Cr/Au (5 nm/50 nm) pad is patterned as the counter electrode for the device. **b**. The α-MnO_2 nanowire is deposited on the 300 nm SiO_2 grown on the Si substrate. **c**. The α-MnO_2 nanowire is immobilized by the electron-beam lithography followed by the Cr/Au (5 nm/150 nm) deposition. **d**. The passivation layer (SU-8) is patterned to cover the Cr/Au electrode using the electron-beam lithography. **e**. A PDMS microfluidic chip is used to confine the electrolyte. The 6 mol/L KOH electrolyte is injected into the device and covers the working electrode (α-MnO_2 nanowire) and the Cr/Au counter electrode. **f**. For the three-electrode electrochemical measurements, the SCE reference electrode is integrated into the device via a channel in the PDMS chip which connects directly to the electrolyte.

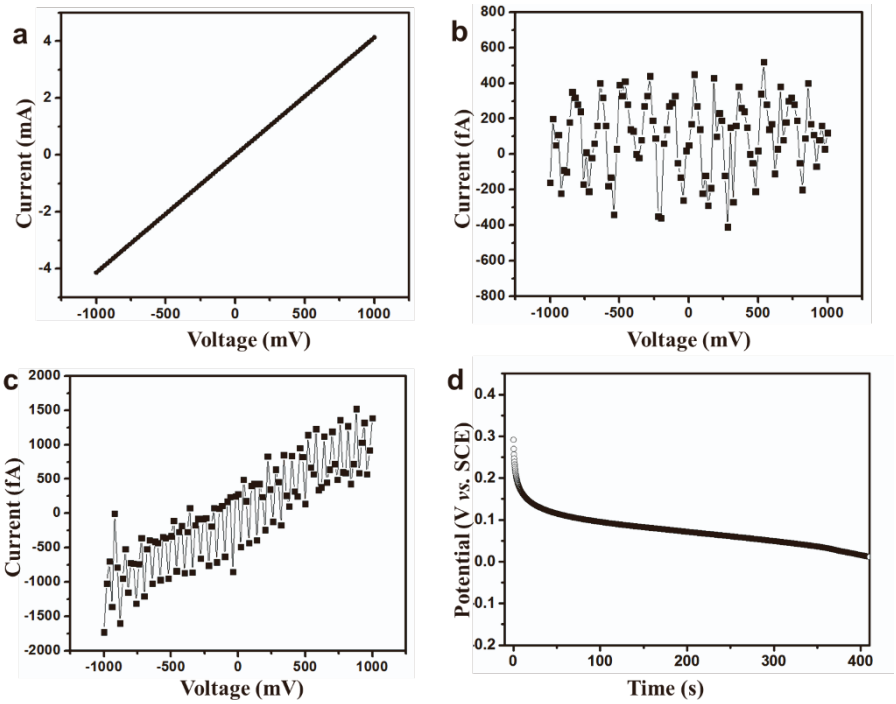

Figure S2. Leakage current experiment. The I-V curves for **(a)** the gold electrodes, **(b)** the SU-8 isolation layer, **(c)** the 300 nm SiO_2 dielectric layer, and **(d)** the self-discharge curve of α-MnO_2 nanowire after charging to 0.4 V *vs.* SCE in the 6M KOH electrolyte. Leakage currents from the single nanowire devices were investigated in two areas. The first one is the SiO_2 dielectric layer. In this case, a 300 nm thick SiO_2 dielectric layer covers the conductive Si wafer. The SiO_2 dielectric layer is widely used in microelectronics, and is known to be an excellent insulator with a leakage current of less than 5 pA.[1] Similar behavior is shown in the experiment here as leakage currents up to 0.5 pA are observed (Fig. S2b). Another possible current source leakage is the current collector with the SU-8 passivation layer. The SU-8 is another high-quality dielectric material that has been widely used in detectors and biosensors.[2] In our system, it leads to a leakage current of ~0.15 nA which is at least 10 times lower than the electrochemical responses shown in Fig. S2c. In addition, we have investigated the total leakage current of the device. Using a three-electrode configuration, we charged the α-MnO_2 nanowire to 0.4 V vs. SCE and monitored the self-discharge behavior. Based on the CV curves in Figure 2a, the discharge plateau should appear at ~0 V vs. SCE. The self-discharge curve for the α-MnO_2 nanowire after charging to 0.4 V vs. SCE in the 6M KOH electrolyte is shown in Figure S2d. The self-discharge plateau starts at ~0.1 V vs. SCE, and the potential approaches ~ 0 V after 400 s. Taking the stored charge of a single α-MnO_2 nanowire (d = 30 nm, l = 20 μm) at ~1×10^{-9} C, the average leakage current of the system immersed in a 6 M KOH solution is ~5 pA. We further calculated the energy consumption of the FE-ESD with a gate-voltage of 3 V. As shown in Figure S2c, the leakage current across the SiO_2 dielectric layer is around 1.5 pA at 1 V. If consider the 300 nm SiO_2 as a resistance with a specific resistance of 1 V / 1.5 pA = 6.7E11 Ω. The leakage current at 3 V gate-voltage will be 7.5 pA. The corresponding energy consumption is about 3 V × 7.5 pA = 2.25 pW for a nanowire-based, field-effect energy storage device.

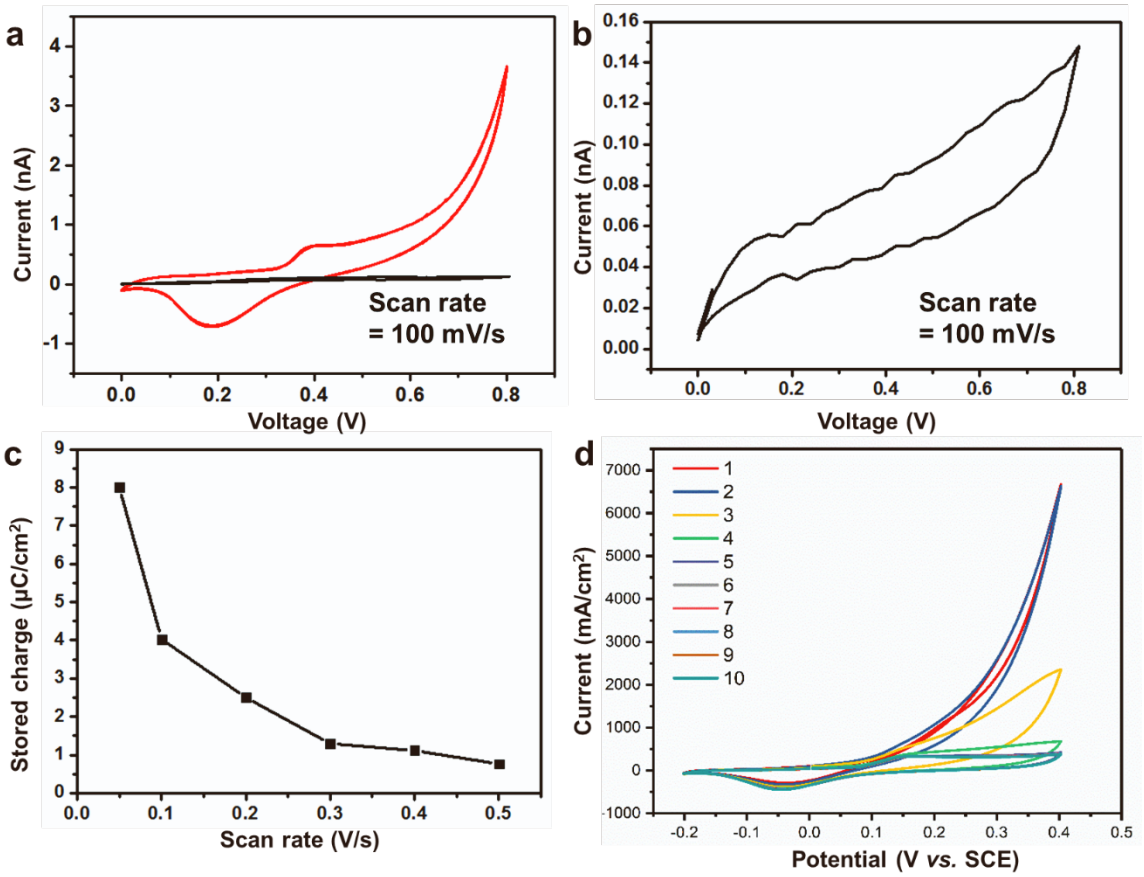

Figure S3. The leakage current measurements at varied conditions. a. CV curves for FE-ESD with (red line) and without (black line) the α-MnO_2 nanowire cathode at the scan rate of 100 mV/s. **b**. The magnified CV curve for the FE-ESD without the cathode (i.e., current flow through the electrolyte). **c**. The stored charge of the FE-ESD without electrode material at scan rates of 50, 100, 200, 300, 400, and 500 mV/s. These results prove that the stored charge of the single α-MnO_2 nanowire FE-ESD comes primarily from the α-MnO_2 nanowire. **d.** CV curves from 1st to 10th cycles with the potential range of -0.2 to 0.4 V *vs.* SCE at 50 mV/s.

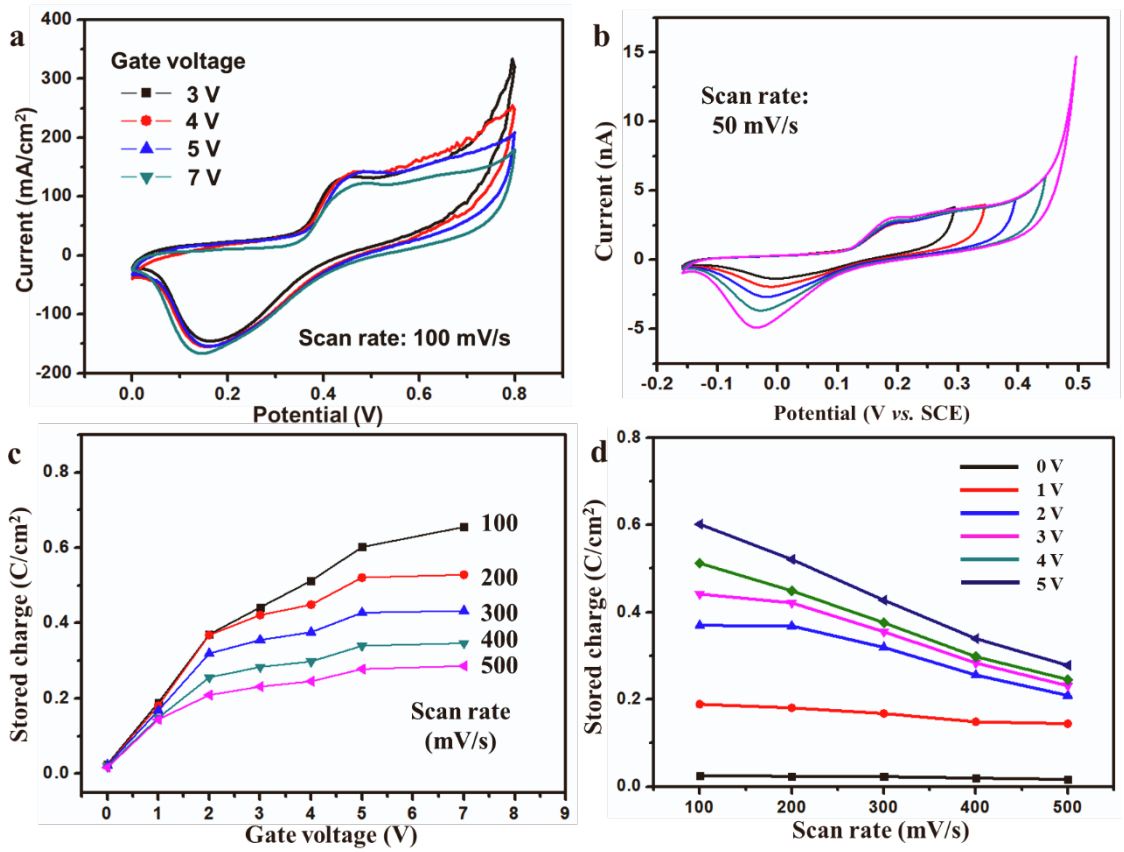

Figure S4. The CV measurements on α-MnO_2 single nanowire FE-ESD (two-electrode configuration). **a**. CV curves (two-electrode configuration) of the α-MnO_2 single nanowire FE-ESD at 100 mV/s with the gate-voltages of 3, 4, 5, and 7 V. **b**. CV curves (three-electrode configuration) at 50 mV/s showing the influence of the potential-window. **c.** The stored charge determined in a three-electrode configuration for the single α-MnO_2 nanowire FE-ESD as a function of gate-voltage (0 – 7 V; calculated based on three-electrode configuration results). **d.** The stored charge determined in a three-electrode configuration for the single α-MnO_2 FE-ESD as a function of the scan rate (100 – 500 mV/s; calculated based on three-electrode configuration results).

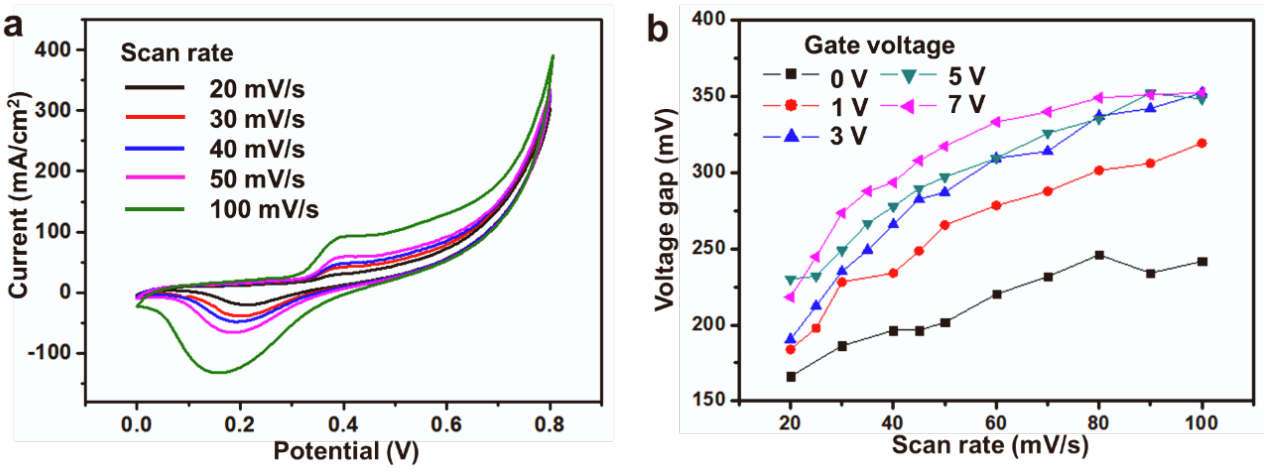

Figure S5. The CV measurements on α-MnO_2 single nanowire device without a back-gate-voltage. a. CV curves of the α-MnO_2 single nanowire device without a back-gate-voltage at the scan rates of 20, 30, 40, 50, and 100 mV/s. **b.** The voltage gap between the anodic and cathodic peaks of the CV curves as a function of the scan rate.

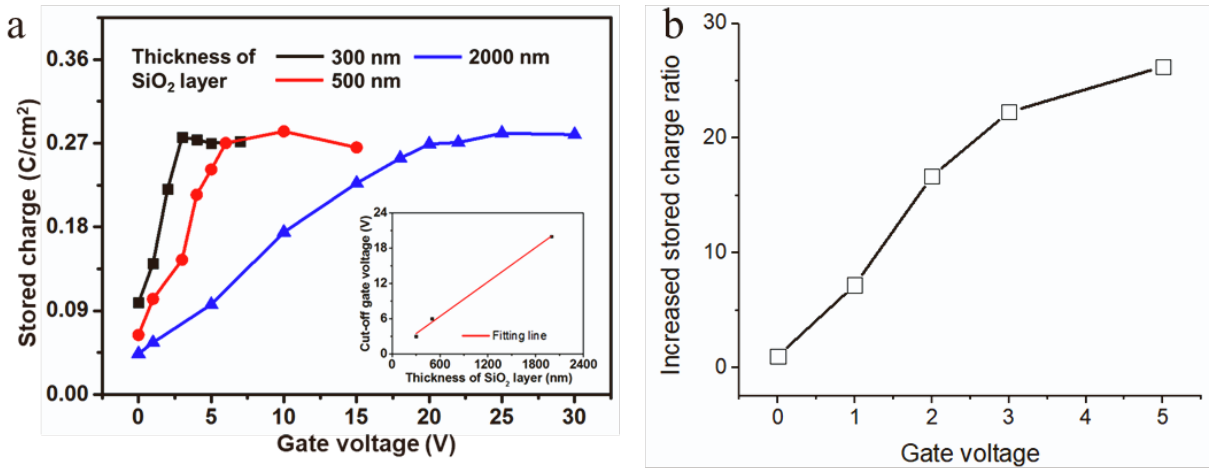

Figure S6. **The SiO_2 thickness effect on FE-ESD performance and the FE-ESD in a poly(vinyl alcohol)-KOH polymer solid electrolyte.** (a) The FE-ESD performance *vs.* gate voltage with varies dielectric layer (SiO_2) thicknesses at a scan rate of 100 mV/s. The inset shows the cut-off voltage *vs.* dielectric layer thickness. The effect of dielectric-layer (SiO_2) thickness on the FE-ESD performance was also investigated (Fig. S8). With increasing gate voltage, the stored charge of the MnO_2 nanowire initially increases and then levels off, regardless of the SiO_2 thickness. Additionally, there is a linear relationship between the dielectric layer thickness and the cut-off voltage of MnO_2 nanowires. (b) The increased stored charge ratio of the MnO_2 nanowire in a poly(vinyl alcohol)-KOH polymer solid electrolyte after applying the gate voltage.

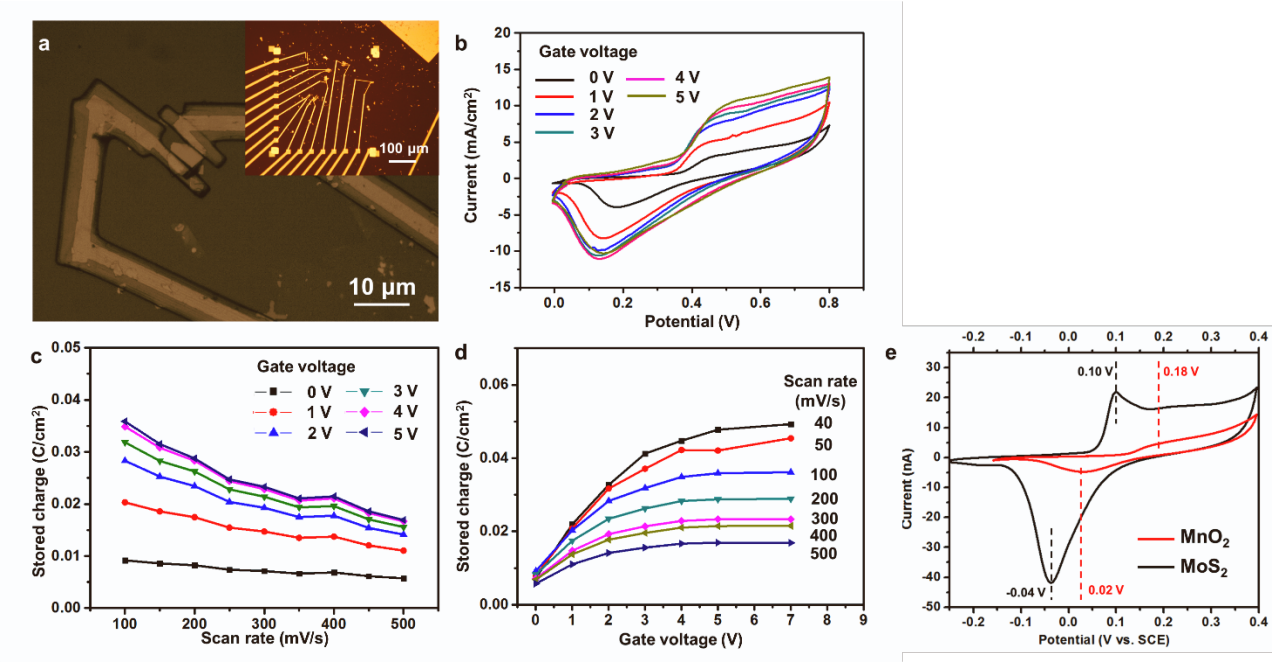

Figure S7. **The performance of MoS_2 nanosheet FE-ESD. a.** An optical image in which a MoS_2 nanosheet is in contact with electrodes and covered by SU-8 to avoid leakage (inset is a typical field effect modulated nanosheet energy storage device). **b**. CV curves of the MoS_2 sheet at the gate-voltages of 0 – 5 V with a scan rate of 100 mV/s. **c.** The stored charge of the MoS_2 nanosheet FE-ESD as a function of the scan rate (100 – 500 mV/s) for different gate-voltages. **d**. The stored charge of the MoS_2 nanosheet FE-ESD as a function of the gate-voltage (0 – 7 V) at various scan rates. **e.** CV curves for single α-MnO_2 nanowire and MoS_2 nanosheet devices taken at the scan rate of 50 mV/s without the gate-voltage. For MoS_2, the oxidation and reduction peaks are located at -0.04 and 0.10 V *vs.* SCE, respectively. For the α-MnO_2 nanowire, redox peak positions are located at 0.02 and 0.18 V *vs.* SCE (see also Fig. S4b), different from those of the MoS_2 sheets.

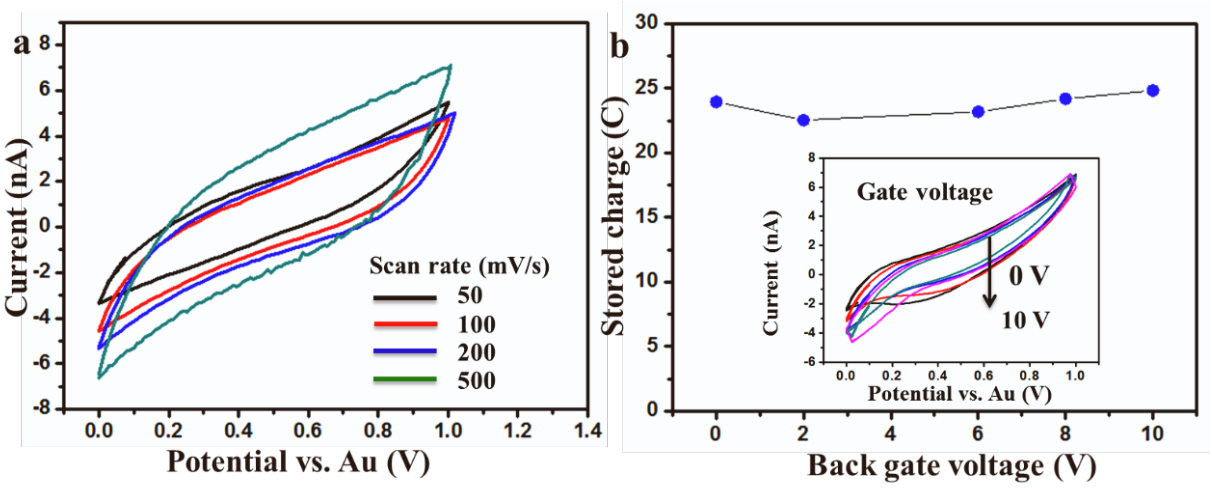

Figure S8. The performance of single graphene sheet-based FE-ESD a. CV curves for the single graphene sheet without the gate voltage at scan rates of 50, 100, 200 and 500 mV/s. **b.** The stored charge of the single graphene sheet at gate voltages of 0, 2, 6, 8, 10 V at a scan rate of 100 mV/s. In this case the gate voltage has no effect. The CV curves at different gate voltages are shown in the inset.

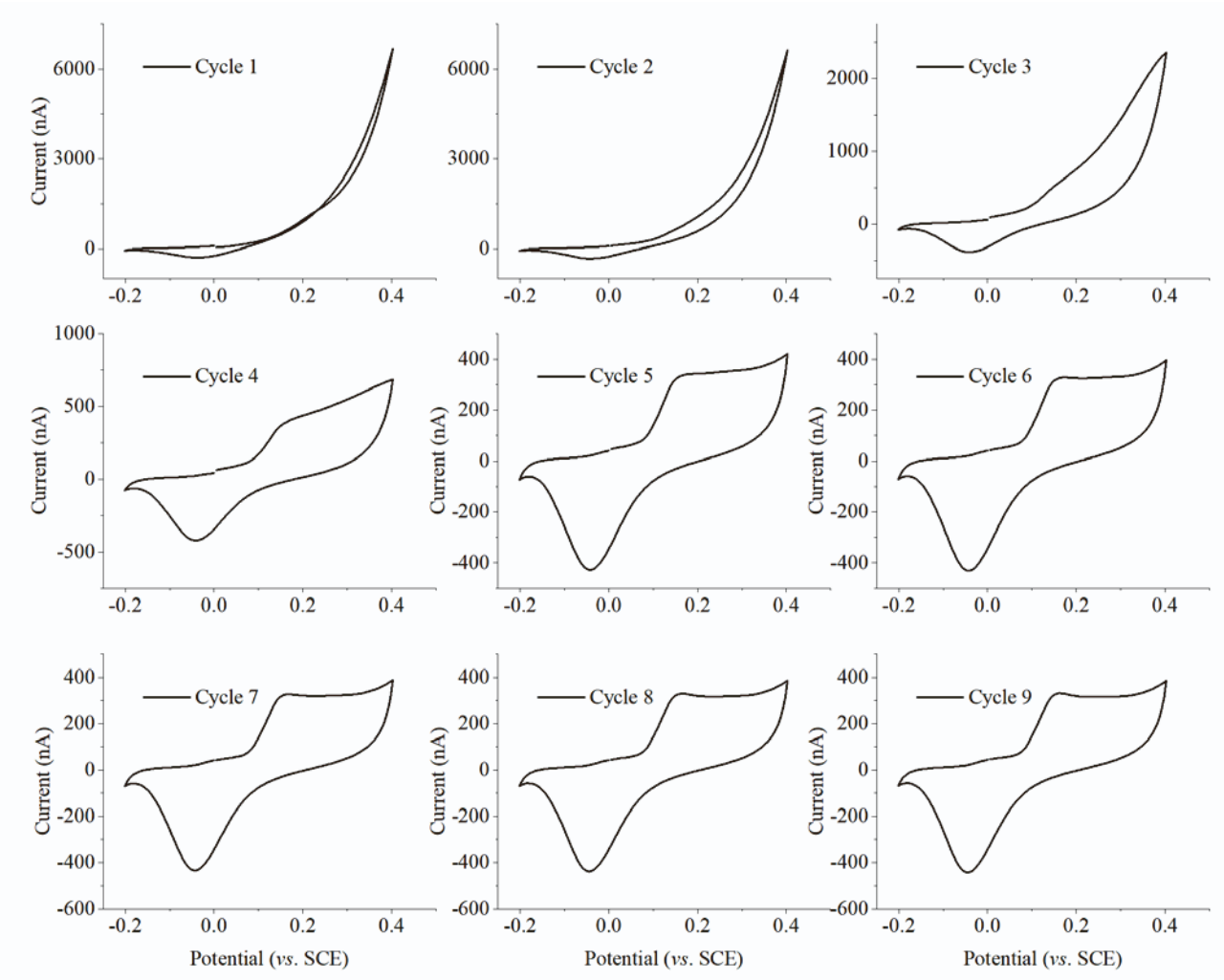

Figure S9. **The separated CV cycles.** The separated CV curves from 1st to 10th cycles with the potential range of -0.2 – 0.4 V *vs.* SCE at 50 mV/s.

Part 3: CV simulation

1. Electrode band bending calculation

With induced different gate-voltages, the experimental OCP values (denoted as V_{OCP}) of MnO_2 electrode shown variations, changing from -0.25 V (vs. SCE) at gate-voltage of 0 V to -1.7 V (vs. SCE) at gate-voltage of 3 V (Figure 4a). Here, we consider the OCP value of MnO_2 as Fermi level of electrode without influence of electrolyte (Figure 4b). Once focusing on the electrode interface region contacting with electrolyte, there would leading to a band-bending of MnO_2 electrode. This is because the Fermi level of electrode at interface of electrode/electrolyte is fixed (denoted as $V_{surface}$) and its value is deviated from OCP values. For different OCP values under each gate-voltage, the electrode band-bending profiles closing the electrode/electrolyte interface will also be changed. To quantitatively describe them, we carried out a 1D model based on the classic Poisson-Boltzmann equation:

$$\nabla \cdot (\epsilon_0 \epsilon_r \nabla \phi_E) = c_0 (\exp\left(-\frac{e\phi_E}{k_B T}\right) - \exp\left(\frac{e\phi_E}{k_B T}\right)) \quad (1)$$

where ϕ_E is the electric potential (i.e., Fermi level) of electrode, ϵ_0 is the vacuum permittivity, ϵ_r is the relative permittivity of the MnO_2 electrode, which is set as 68 referred from literature[3]. c_0 is the bulk concentration of charge carriers in MnO_2 electrode (i.e., electron and hole)[4], which is set as 3.46 $\times 10^{24}$ 1/m^3. e is the elementary charge. k_B is the Boltzmann constant and T is the temperature and equals to 300 K in this work.

The boundary conditions were added at the two ends of 1D model: $\phi_E\,(x = 0) = 0$ V and $\phi_E(x = L) = V_{surface} - V_{OCP}$ with L=30 nm according to the diameter of MnO_2 nanowire. Here, we using finite-element method calculated two band-bending profiles for V_{OCP} = -0.25 V/$V_{surface}$ = -1.119 V vs. SCE at gate voltage of 0V and V_{OCP} = -1.7 V/$V_{surface}$ = -1.119 V vs. SCE at gate voltage of 3 V, respectively. Figure S10 presents the band-bending profiles (blue lines) of electrode Fermi level at contacting with electrolyte. We can observe the reverse band bending directions when gate voltages change from 0 V to 3 V, which would lead to different shifts of equilibrium potentials for H^+ intercalation into MnO_2 electrode from standard value. To estimate the shift ranges of equilibrium potentials for H^+ intercalation, we involved H^+ energy level and the potential window of CV measurement (red line and grey region). It shows that at each gate voltage induced condition, the electric potential range during CV process for H^+ accessible intercalations are varied. Via averaging the H^+ accessible potential levels, the equilibrium potential of H^+ is estimated to be -0.051 V at gate of 0 V and 0.297 V at gate voltage of 3 V.

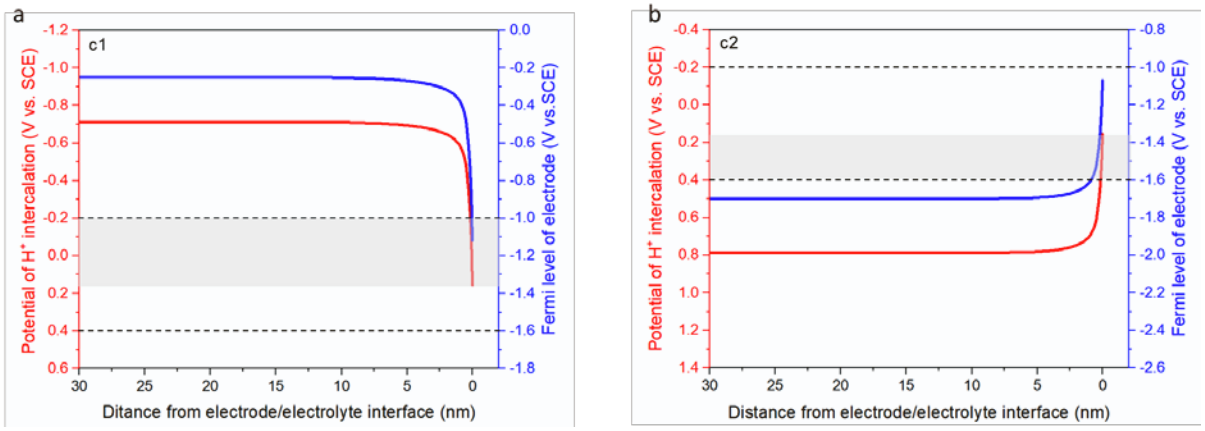

Figure S10. Diagram of band-bending of electrode Fermi-level at interfacial region closing to electrolyte for c1 region labelled in Figure 4e (a) and c3 region (b).

2. Cyclic voltammetry curves at different band-bending conditions

To study how CV curves particularly the redox peaks of MnO_2 electrode will response to the shifted equilibrium potentials of H^+ intercalation, we further simulate the CV process using an interfacial model, where the redox reactions and EDL capacity were assumed to happen at electrode surface with estimated overall equilibrium potentials. The single MnO_2 nanowire electrode based electrochemical system was modelled as a representative one-dimensional system. As same with experimental protocols, the cyclic voltammetry (CV) process was simulated for studying the variations of electrochemical reaction.

The redox reaction on MnO_2 cathode in this work is based on following chemical equation:

$$x\mathrm{OH^-} + \mathrm{H}_y\mathrm{MnO_2} = \mathrm{H}_{y-x}\mathrm{MnO_2} + x\mathrm{H_2O} + e^- \quad (2)$$

The modelling contains a single 1D domain of length L_l, which is set as ~2 mm, greatly exceeding diffuse layer at electrified surface under the context that the practical electrolyte is sufficient for single MnO_2 nanowire electrolyte.

2.1Domain equations

Considering the practical electrode used in experiment is 6M KOH aqueous electrolyte, in the domain where the electrolyte is accessible, the diffusion equation (i.e., Fick's 2nd law) and Poisson equation were adopted to describe the local concentration of the electroactive species $c_i(x,t)$ with i = K^+, OH^- and H^+ species and electric potential in the electrolyte $\phi_l(x,t)$:

$$\frac{\partial c_i}{\partial t} = \nabla \cdot (D_i \nabla c_i), \quad (3)$$

$$-\nabla \cdot (\epsilon_0 \epsilon_r \nabla \phi_l) = F(z_{\mathrm{K^+}} c_{\mathrm{K^+}} + z_{\mathrm{OH^-}} c_{\mathrm{OH^-}} + z_{\mathrm{H^+}} c_{\mathrm{H^+}}) \quad (4)$$

where ϵ_0 and ϵ_r are the vacuum permittivity and the relative permittivity of the electrolyte, respectively. F is the Faraday constant. D_i is the diffusion coefficient of species. $z_{\mathrm{K^+}}$, $z_{\mathrm{H^+}}$ and $z_{\mathrm{OH^-}}$ are the charge valence of K^+ ion, OH^- ion, H^+ ion, respectively. Note that here we consider a considerable amount of H^+ in alkaline electrolyte because: 1) it has been widely documented that H^+ is main species for redox reactions in MnO_2 electrode even in alkaline electrolyte[5]; 2) there are obvious redox peaks characterised in experiments where considerable amount of H^+ is expected. There is no detailed mechanism being developed for H^+ source. Some literature indicated that the interfacial water dissociation may have a contribution.

2.2 Boundary conditions

At the boundary representing electrode/electrolyte interface where redox reaction would happen ($x = 0$), charge conservation was adopted where the electronic current density at the electrode/electrode interface equals to the sum of the electrochemical intercalation current density i_{loc} and electric double layer (EDL) capacitive current i_{EDL}:

$$i_{\mathrm{total}} = i_{\mathrm{loc}} + i_{\mathrm{EDL}} \quad (5)$$

The intercalation current density i_{loc} is determined by the general form of Butler-Volmer (BV) equation for a one-electron transfer reaction, which is applicable to the mass transfer influenced conditions:

$$i_{\mathrm{loc}} = i_0 \left(\frac{c_{\mathrm{OH^-}}}{c^{\mathrm{b}}_{\mathrm{OH^-}}} \exp\left(\frac{(1-\alpha)F\eta}{RT}\right) - \frac{c_{\mathrm{H^+/MnO_2}}}{c^{\mathrm{b}}_{\mathrm{H^+/MnO_2}}} \exp\left(\frac{-\alpha F\eta}{RT}\right) \right) \tag{6}$$

Where i_0 is the exchange current density. α is the transfer coefficient, which is taken as 0.5 in this work corresponding to the identical energy barriers for the forward and backward redox reactions. η is the overpotential at the working electrode, which represents the deviation of the electric potential drop across electrode/electrolyte interface and the equilibrium potential of the redox couple of species, $\eta = \phi_{\mathrm{S}} - \phi_l - E_{\mathrm{eq}}$. Here, the E_{eq} value at different gate-voltage is adopted based on section 1 results.

The EDL capacitive current i_{EDL} was described as:

$$i_{\mathrm{EDL}} = C_{\mathrm{EDL}} \frac{\partial(\phi_S - \phi_l)}{\partial t} \tag{7}$$

At the bulk boundary ($x = L$), the concentration constraints are set as the concentration of reactant and K^+ species equal to the bulk concentration c_0 and zero concentration is set for product species:

$$c_{\mathrm{OH^-}} = c_{\mathrm{K^+}} = c_0 \tag{8a}$$

$$c_{\mathrm{H^+}} = 0 \tag{8b}$$

Under cyclic voltammetry (CV) process, the voltage was imposed at the surface boundary ($x = 0$)

$$\phi_S = \phi_{\mathrm{app}} = \begin{cases} \mathrm{V_{min}} + vt & \text{For charging } 2n\tau < t < (2n+1)\tau \\ \mathrm{V_{max}} - v(t-\tau) & \text{For discharging } (2n+1)\tau < t < 2(n+1)\tau \end{cases} \tag{9}$$

where $\mathrm{V_{min}}$ and $\mathrm{V_{max}}$ are the lowest and highest voltage value of potential window, respectively. v is the scan rate of the cyclic voltammetry as in experimental value. τ is the time duration of half charging cycle $\tau = (\mathrm{V_{max}}\text{-}\mathrm{V_{min}})/v$. n=1, 2, 3… is the cycle number.

2.3 Initial conditions

The initial electric potential was set as uniform and equal to zero across the domain as

$$\phi_l(x, 0) = 0\ \mathrm{V} \tag{10}$$

The initial species concentrations were uniform with bulk concentration

$$c_{\mathrm{OH^-}} = c_{\mathrm{K^+}} = c_0 \text{ and } c_{\mathrm{H^+}} = 0 \tag{11}$$

2.4 Constitutive relationships

Consider the practical electrolyte is 6 mol/L KOH, the relative permittivity of the electrolyte ϵ_r = 80 was adopted. The diffusion coefficients of K^+ and OH^- were adopted as $D_{\mathrm{K^+}}$ = 1.957×10^{-5} cm^2 s^{-1}, $D_{\mathrm{H^+}}$ = 9.3 ×10^{-5} cm^2 s^{-1} and $D_{\mathrm{OH^-}}$ = 5.28×10^{-5} cm^2 s^{-1}, respectively[6]. C_{EDL} = 6 μF/cm^2, which is in typical aqueous electric double layer capacitance ranges.

V_{min} = -0.2 V vs. SCE and V_{max} = 0.4 V vs. SCE have been adopted based on practical measurement. The scan rate v = 0.001 V/s is adopted. The equilibrium potential E_{eq} is adopted as -0.051 V *vs*. SCE at gate voltage of 0 V and 0.297 V vs. SCE at gate voltage of 3 V. i_0 was adopted as 10 A/m^2. $c^b_{OH^-}$ = 6M and $c^b_{H^+/MnO_2}$ = 1M are adopted (Figure S11).

2.5 Results

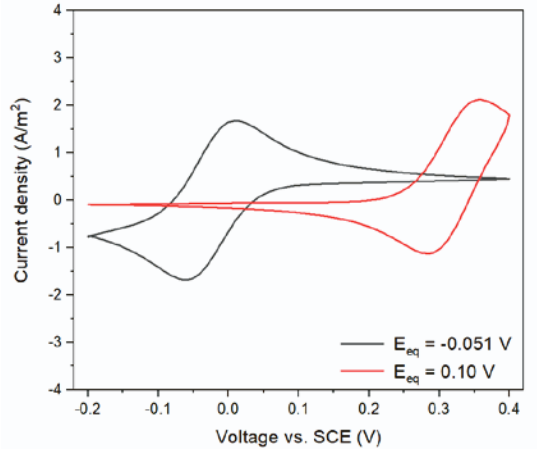

Figure S11. CV curves of MnO_2 electrode at different gate-voltages.

Supplemental references:

1. Javey, A., Guo, J., Wang, Q., Lundstrom, M., and Dai, H. (2003). Ballistic carbon nanotube field-effect transistors. Nature *424*, 654-657. https://doi.org/10.1038/nature01797.
2. Kim, H., Plis, E., Khoshakhlagh, A., Myers, S., Gautam, N., Sharma, Y., Dawson, L., Krishna, S., Lee, S., and Noh, S. (2010). Performance improvement of InAs/GaSb strained layer superlattice detectors by reducing surface leakage currents with SU-8 passivation. Applied Physics Letters *96*, 033502. https://doi.org/10.1063/1.3275711.
3. Moalleminejad, M., and Chung, D. (2015). Dielectric constant and electrical conductivity of carbon black as an electrically conductive additive in a manganese-dioxide electrochemical electrode, and their dependence on electrolyte permeation. Carbon *91*, 76-87. https://doi.org/10.1016/j.carbon.2015.04.047.
4. Hedden, M., Francis, N., Haraldsen, J.T., Ahmed, T., and Constantin, C. (2015). Thermoelectric properties of nano-meso-micro β-MnO_2 powders as a function of electrical resistance. Nanoscale Research Letters *10*, 1-9. https://doi.org/10.1186/s11671-015-1000-6.
5. Lévy-Clèment, C., Mondoloni, C., Godart, C., and Cortès, R. (1990). In Situ X-Ray Diffraction and In Situ X-Ray Absorption Spectroscopy for Investigation of Intercalation Batteries: Application to the Alkaline H^+/γ-MnO_2 system. MRS Online Proceedings Library *210*. https://doi.org/10.1557/PROC-210-387.
6. Samson, E., Marchand, J., and Snyder, K.A. (2003). Calculation of ionic diffusion coefficients on the basis of migration test results. Materials and Structures *36*, 156-165. https://doi.org/10.1007/BF02479554.